
Topological Relational Learning on Graphs

Yuzhou Chen

Department of Electrical Engineering
Princeton University
yc0774@princeton.edu

Baris Coskunuzer

Department of Mathematical Sciences
University of Texas at Dallas
coskunuz@utdallas.edu

Yulia R. Gel

Department of Mathematical Sciences
University of Texas at Dallas
ygl@utdallas.edu

Abstract

Graph neural networks (GNNs) have emerged as a powerful tool for graph classification and representation learning. However, GNNs tend to suffer from over-smoothing problems and are vulnerable to graph perturbations. To address these challenges, we propose a novel topological neural framework of topological relational inference (TRI) which allows for integrating higher-order graph information to GNNs and for systematically learning a local graph structure. The key idea is to rewire the original graph by using the persistent homology of the small neighborhoods of nodes and then to incorporate the extracted topological summaries as the side information into the local algorithm. As a result, the new framework enables us to harness both the conventional information on the graph structure and information on the graph higher order topological properties. We derive theoretical stability guarantees for the new local topological representation and discuss their implications on the graph algebraic connectivity. The experimental results on node classification tasks demonstrate that the new TRI-GNN outperforms all 14 state-of-the-art baselines on 6 out of 7 graphs and exhibit higher robustness to perturbations, yielding up to 10% better performance under noisy scenarios.

1 Introduction

Node classification is one of the most active research areas in graph learning. The target here is, given a single attributed graph \mathcal{G} and a small subset of nodes with prior label information, to predict labels of all remaining unlabelled nodes. Applications of node classification are very diverse, ranging from customer attrition analytics to tracking corruption-convictions among politicians. Graph neural networks (GNNs) offer a powerful machinery for addressing such problems on large heterogeneous networks, resulting in an emerging field of geometric deep learning (GDL) which adapts deep learning to non-Euclidean objects such as graphs [9, 56, 59, 17].

Although GDL achieves a highly competitive performance in various graph-based classification and prediction tasks, similarly to the image domain deep learning on graphs is often found to be vulnerable to graph perturbations and adversarial attacks [46, 55, 28]. In turn, most recent results [45, 21] suggest that local graph information may be invaluable for robustifying GDL against graph perturbations and adversarial attacks. Also, as shown by [38, 4, 58] in conjunction with network community learning, local algorithms (i.e., algorithms based only on a small radius neighborhood around the node) may demonstrate superior performance if coupled with side information in the form of a node labeling positively correlated with the true graph structure. Inspired by these results, the ultimate goal of this paper is to introduce the idea of local algorithms with *local topological side information* on similarity

of node neighborhood shapes into GNN. By *shape* here, we broadly understand data characteristics which are invariant under continuous transformations such as stretching, bending, and compressing, and to study such graph shapes properties, we invoke the machinery of topological data analysis (TDA) [23, 11].

Topological Relational Inference: from Matchmaking to Adversarial Graph Learning and Beyond In particular, to capture more complex graph properties and enhance model robustness, we introduce the concept of topological relational inference (TRI) and propose two novel options for information passing which rely on the local topological structure of each node: (i) Inject a new topology-induced multiedge between two nodes based on shape similarity of their local neighborhoods; (ii) Enrich each individual node features by harnessing local topological side information from its neighbors. The rationale behind our idea is multi-fold. First, we assess not only global graph topology and relationships between the feature sets of two individual nodes, as with the current diffusion mechanisms and random walks on graphs, but we also examine important *interactions between shapes of the feature sets of the node neighborhoods*. As a result, our new topology-induced multigraph representation (TIMR) of graph \mathcal{G} in (i) strengthens the relationship among nodes which might not be (yet) connected by a visible (or "tangible") edge in \mathcal{G} but whose higher order intrinsic characteristics are very similar. The intuitive analogy here might be with a matchmaking agency who aims to connect two people on a blind date, based on a careful assessment of interplay among similarities of their interests, socio-demographics as well as that of their close friends, rather than bringing in two individuals together through a random walk among all available profiles of potential candidates. Another example is the customer churn and retention analytics based on peer effects [16]. That is, the goal here is to classify the node as potential churn customer based not only on the individual attributes but on interactions among its neighbor attributes. Second, such a new multiedge in (i), based on shape similarity of node local neighborhoods may assist not only the matchmaking agency in coupling the most appropriate individuals (or link prediction in less romantic and more technical terms), but to enhance resilience of the graph structure and associated graph learning. Indeed, a new multiedge in (i) can be used as an essential remedial ingredient in graph defense mechanisms as criteria to clean the perturbed graph, i.e., to reconstruct edges removed by the attacker or to suppress edges induced by the attacker, depending on the strength of the topology-induced link. Third, by learning shape properties within each local node neighborhood, our TRI allows for systematic recovering of intrinsic higher-order interactions among nodes well beyond a level of pair-wise connectivity, and such local topological side information in (ii) enhances accuracy in node classification tasks even on clean graphs. Significance of our contributions are the following:

- We propose a novel perspective to graph learning with GNN – topological relational inference, based on the idea of similarity among shapes of local node neighborhoods.
- We develop a new topology-induced multigraph representation of graphs which systematically accounts for the key local information on the attributed graphs and serves as an important remedial ingredient against graph perturbations and attacks.
- We derive theoretical stability guarantees for the new local topological representation of the graph and discuss their implications for the graph algebraic connectivity.
- Our expansive node classification experiments show that TRI-GNN outperforms 14 state-of-the-art baselines on 6 out of 7 graphs and delivers substantially higher robustness (i.e., up to 10% in performance gains under noisy scenarios) than baselines on all 7 datasets.

2 Related Work

Graph Neural Networks Inspired by the success of the convolution mechanism on image-based tasks, GNNs continue to attract an increasing attention in the last few years. Based on the spectral graph theory, [10] introduced a graph-based convolution in Fourier domain. However, complexity of this model is very high since all Laplacian eigenvectors are needed. To tackle this problem, ChebNet [20] integrated spectral graph convolution with Chebyshev polynomials. Then, Graph Convolutional Networks (GCNs) of [32] simplified the graph convolution with a localized first-order approximation. More recently, there have been proposed various approaches based on accumulation of the graph information from a wider neighborhood, using diffusion aggregation and random walks. Such higher-order methods include approximate personalized propagation of neural predictions (APNP) [33], higher-order graph convolutional architectures (MixHop) [3], multi-scale graph

convolution (N-GCN) [2], and Lévy Flights Graph Convolutional Networks (LFGCN) [15]. In addition to random walks, other recent approaches include GNNs on directed graphs (MotifNet) [37], graph convolutional networks with attention mechanism (GAT, SPAGAN) [51, 57], and graph Markov neural network (GMNN) [41]. Most recently, Liu et al. [36] consider utilizing information on the node neighbors’ features in GNN, proposing Deep Adaptive Graph Neural Network (DAGNN). However, DAGNN does not account for the important information on the shapes of the node neighborhoods.

Persistent Homology for Graph Learning Machinery of TDA and persistent homology (PH) is increasingly widely used in conjunction with graph classification, that is, when the goal is to predict a label for the entire graph rather than for individual nodes. Such tools for graph classification with persistent topological signatures include kernel-based methods [49, 42, 35, 60, 34] and neural networks [26, 12]. All of the above methods consider the task of classifying graph labels and are based on assessing ‘global’ graph topology, while our focus is node classification and our approach is based on evaluating local topological graph properties (i.e., shape of individual node neighborhoods). Integration of PH to node classification is virtually unexplored. To the best of our knowledge, the closest result in this direction is PEGN-RC [61]. However, the key idea of PEGN-RC is distinctly different from our approach. PEGN-RC reweights **only each existing edge**, based on the topological information within its edge vicinity and, in contrast to TRI-GNN, neither compares any shapes, nor creates new or removes existing edges. Importantly, PEGN-RC does not integrate topology of both graph and node attributes, while TRI-GNN does.

3 Preliminaries on Topological Data Analysis and Persistent Homology

The machinery of topological data analysis (TDA) and, particularly, persistent homology offer a mathematically rigorous and systematic framework of tools to evaluate shape properties of the observed data, that is, intrinsic data characteristics which are invariant under continuous deformations such as stretching, compressing, and bending [63, 23, 39]. The main premise is that the observed data which can be, as in our case, a graph \mathcal{G} or a point cloud in a Euclidean or any finite metric space constitute a discrete sample from some unknown metric space \mathcal{M} . Our goal is then to recover information on some essential properties of \mathcal{M} which has been lost due to sampling. Persistent homology addresses this reconstruction task by counting occurrences of certain patterns, e.g., loops, holes, and cavities, within shape of \mathcal{M} . Such pattern counts and functions thereof, called *topological signatures* are then used to characterize intrinsic properties of \mathcal{G} .

The approach is implemented in two main steps. We start from associating \mathcal{G} with some nested sequence of subgraphs $\mathcal{G}_1 \subseteq \mathcal{G}_2 \subseteq \dots \subseteq \mathcal{G}_m = \mathcal{G}$. Then we monitor evolution of pattern occurrences (e.g., cycles, cavities, and more generally n -dimensional holes) in this nested sequence of subgraphs. To ensure a systematic and computationally efficient manner of pattern counting, we construct a simplicial complex \mathcal{C}_i (e.g., a clique complex) induced by \mathcal{G}_i . The sequence $\{\mathcal{G}_i\}$ induces a *filtration*: nested sequence of simplicial complexes $\mathcal{C}_1 \subseteq \mathcal{C}_2 \subseteq \dots \subseteq \mathcal{C}_m = \mathcal{C}$. Now we can not only track patterns but also evaluate the lifespan of each topological feature. Let b_σ be the index of the simplicial complex \mathcal{C}_{b_σ} at which we first record (i.e., birth) the n -dimensional topological feature σ (n -cycle), while simplicial complex \mathcal{C}_{d_σ} be the first complex we observe its disappearance (i.e., death). Then lifespan or *persistence* of the topological feature σ is $d_\sigma - b_\sigma$. To evaluate all topological features together, we consider a *persistence diagram (PD)* where the multi-set $\mathcal{D}_n = \{(b_\sigma, d_\sigma) \in \mathbb{R}^2 : d_\sigma > b_\sigma\} \cup \Delta$ records the birth and deaths of all n -cycles in the filtration $\{\mathcal{C}_i\}$. Here, $\Delta = \{(t, t) | t \in \mathbb{R}\}$ is the diagonal set containing points in PD, counted with infinite multiplicity. Different persistent diagrams can be compared based on the cost of the optimal matching between points of the two diagrams, while avoiding topological noise near Δ [13].

Depending on the question at hand, we can construct different suitable filtrations relevant to the problem. In this paper, we consider two different filtrations. First, we consider the sublevel filtration based on a node degree function $f : \mathcal{V} \mapsto \mathbb{N}$. As degree is an integer valued function, so are our thresholds $\{\alpha_i\} \subset \mathbb{N}$. Our sublevel filtration is then defined as follows. Let $\mathcal{V}_{\alpha_i} = \{u \in \mathcal{V} | f(u) \leq \alpha_i\}$. Then, \mathcal{G}_{α_i} is the subgraph generated by \mathcal{V}_{α_i} . In particular, the edge $e_{uv} \in \mathcal{E}$ is in \mathcal{G}_{α_i} if both u and v are in \mathcal{V}_{α_i} . We call this *degree based filtration*. In addition, we consider a second filtration defined by the edge-weight function on the graph where edge weights are induced by similarity of node attributes. We call this *attribute based filtration* (See Section 4). Note that degree based filtration is induced only by the graph properties, while attribute based filtration is constructed by using the features coming from the observed data.

4 Topological Relational Inference Graph Neural Network (TRI-GNN)

Problem Statement Let $\mathcal{G} = (\mathcal{V}, \mathcal{E})$ be an attributed graph with a set of nodes \mathcal{V} , a set of edges $\mathcal{E} \subseteq \mathcal{V} \times \mathcal{V}$ and $e_{uv} \in \mathcal{E}$ denoting an edge between nodes $u, v \in \mathcal{V}$. The total number of nodes in \mathcal{G} is $N = |\mathcal{V}|$. Let $W \in \mathbb{R}^{N \times N}$ be a $N \times N$ -adjacency matrix of \mathcal{G} such that $\omega_{uv} = 1$ for $e_{uv} \in \mathcal{E}$ and 0 otherwise, and D be a diagonal $N \times N$ -degree matrix with $D_{uu} = \sum_v \omega_{uv}$. For undirected graphs W is symmetric (i.e., $W = W^\top$). To feed in directed graphs into the graph neural network architecture, we set $W' = (W^\top + W)/2$. Finally, each $u \in \mathcal{V}$ is equipped with a set of node features, i.e., $X_u = (X_{u1}, X_{u2}, \dots, X_{uF})$ represents an F -dimensional feature vector for node $u \in \mathcal{V}$, and X is a $N \times F$ -matrix of all node features. Our objective is to develop a robust semi-supervised classifier such that we can predict unknown node labels in \mathcal{G} , given some training set of nodes in \mathcal{G} with prior labeling information. Figure 1 illustrates our TRI-GNN model framework.

4.1 Topology-induced Multigraph Representation

The first step in our TRI model with the associated Topology-induced Multigraph Representation (TIMR) of \mathcal{G} is to define topological similarity among two node neighborhoods. The key goal here is to go beyond the vanilla local optimization algorithms which capture only pairwise similarity of node features [38] and beyond only triangle motifs as descriptors of higher-order node interactions [37, 50]. Our aim is to systematically extract *all* n -dimensional topological features and their persistence in each node neighborhood and then to compare node neighborhoods in terms of their exhibited shapes.

Definition 1 (Weighted k -hop Neighborhood). An induced subgraph $\mathcal{G}_u^k = (\mathcal{V}_u^k, \mathcal{E}_u^k) \subseteq \mathcal{G}$, equipped with an edge-weight function τ induced by similarity of node features in \mathcal{G}_u^k , is called a *weighted k -hop neighborhood* of node $u \in \mathcal{V}$ if: (1) for any $v \in \mathcal{V}_u^k$, the shortest path between u and v is at most k ; (2) edge-weight function $\tau : \mathcal{V}_u^k \times \mathcal{V}_u^k \mapsto \mathbb{R}_{\geq 0}$ is such that for any $v, w \in \mathcal{V}_u^k$ with $e_{vw} \in \mathcal{E}_u^k$, $\tau_{vw} = \|X_v - X_w\|$, where $\|\cdot\|$ is either Euclidean distance (in the case of continuous node features), Hamming distance (in the case of categorical node features), Heterogeneous Value Difference Metric (HVDM) or other distance appropriate for mixed-type data [22]. If $\tau_{vw} \equiv 1$ for any $e_{vw} \in \mathcal{E}_u^k$, \mathcal{G}_u^k reduces to a conventional k -hop neighborhood.

Armed with the edge-weight function τ induced by node attributes (see Definition 1) or with a node degree function, we now compute a sublevel filtration within each node neighborhood and track lifespan of each extracted topological feature, e.g., components, loops, cavities, and n -dimensional holes (see previous section). Here we consider two cases: attribute based filtration (\mathcal{G}_u^k is equipped with an edge-weight function τ based on node attributes) and degree based filtration (\mathcal{G}_u^k is an unweighted graph with $\tau \equiv 1$). We can then compare how topologically similar shapes exhibited by node neighborhoods in terms of Wasserstein distance among their persistence diagrams.

Definition 2. (Topological Similarity among k -hop Neighborhoods) Let $\mathcal{D}(\mathcal{G}_u^k)$ and $\mathcal{D}(\mathcal{G}_v^k)$ be persistence diagrams of the weighted k -hop neighborhood subgraphs \mathcal{G}_u^k and \mathcal{G}_v^k of nodes u and v , respectively. We measure topological similarity between \mathcal{G}_u^k and \mathcal{G}_v^k with Wasserstein distance between the corresponding persistence diagrams as $d_{W,p}(\mathcal{G}_u^k, \mathcal{G}_v^k) = \inf_{\gamma} \left(\sum_{x \in \mathcal{D}(\mathcal{G}_u^k) \cup \Delta} \|x - \gamma(x)\|_p^p \right)^{\frac{1}{p}}$, where $p \geq 1$ and γ is taken over all bijective maps between $\mathcal{D}(\mathcal{G}_u^k) \cup \Delta$ and $\mathcal{D}(\mathcal{G}_v^k) \cup \Delta$, counting their multiplicities. In our analysis we use $p = 1$.

As noted by [38], integrating neighboring nodes whose labeling is positively correlated with the true cluster structure, as a side information to a community recovery process may lead to substantial performance gains. Inspired by these results, we not only inject topological side information into GNN but also distinguish this side information w.r.t. its strength. We propose a new topology-induced multigraph representation of \mathcal{G} , where a multiedge between nodes u and v comprises information on (tangible) connectivity between u and v (i.e., existence of e_{uv}) as well as on strong and weak topological similarity of the local neighborhoods of u and v , irregardless whether e_{uv} exists.

Definition 3. (Topology-induced Multigraph Representation (TIMR)) Consider a graph $\mathcal{G} = (\mathcal{V}, \mathcal{E})$, with $d_{W,p}(\mathcal{G}_u^k, \mathcal{G}_v^k)$ as a measure of topological similarity among two k -hop neighborhoods \mathcal{G}_u^k and \mathcal{G}_v^k , for all $u, v \in \mathcal{V}$ (see Definition 1). Then a topology-induced multigraph representation of \mathcal{G} is defined as $\Omega = (\mathcal{V}, \mathcal{E}^{\text{topo}})$, where $\mathcal{E}^{\text{topo}}$ is a set of multiedges such that for any $u, v \in \mathcal{V}$ and thresholds $\epsilon_1, \epsilon_2 \in \mathbb{R}^+$

$$\mathbb{1}_{uv}^{\text{topo}} = \{ \mathbb{1}_{e_{uv} \in \mathcal{E}}, \mathbb{1}_{d_{W,p}(\mathcal{G}_u^k, \mathcal{G}_v^k) \in [0, \epsilon_1]}, -\mathbb{1}_{d_{W,p}(\mathcal{G}_u^k, \mathcal{G}_v^k) \in [\epsilon_2, \infty)} \}. \quad (1)$$

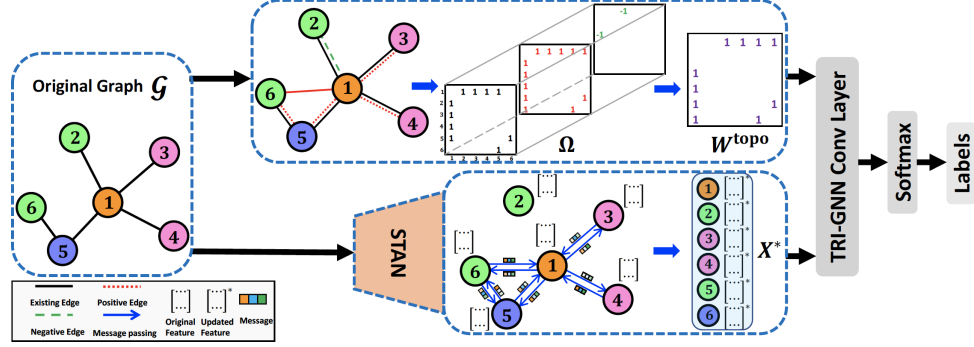


Figure 1: The TRI-GNN semi-supervised learning framework (for more details see Appendix B).

Note that $\{d_{W,p}(\mathcal{G}_u^k, \mathcal{G}_v^k) \in [0, \epsilon_1]\}$ and $\{d_{W,p}(\mathcal{G}_u^k, \mathcal{G}_v^k) \in [\epsilon_2, \infty)\}$ are incompatible events. Hence, multiedges have multiplicity at most 2 and $\mathcal{E}^{\text{topo}}$ is a multiset of $\{(1, 1, 0); (0, 1, 0); (1, 0, -1); (0, 0, -1)\}$. The intuition behind TIMR is to reflect a level of shape similarity among any two node neighborhoods, irregardless whether there exists an edge between these nodes in \mathcal{G} . Later, by using Ω , we induce a graph W^{topo} (Figure 1) defined as follows: If neighborhoods of two nodes in \mathcal{G} are topologically similar, we add an edge between the nodes if there is none. If neighborhoods of two nodes in \mathcal{G} are topologically dissimilar, we remove the edge between the nodes if one exists.

Alternatively, we can associate TIMR with *positive topology-induced* and *negative topology-induced* adjacency matrices, $W^{\text{topo}+}$ and $W^{\text{topo}-}$, respectively

$$W_{uv}^{\text{topo}+} = [0 \leq d_{W,p}^f(\mathcal{G}_u^k, \mathcal{G}_v^k) < \epsilon_1], \quad W_{uv}^{\text{topo}-} = [\epsilon_2 < d_{W,p}^f(\mathcal{G}_u^k, \mathcal{G}_v^k) < \infty], \quad (2)$$

where $[\cdot]$ is an Iverson bracket, i.e., 1 whenever a condition in the bracket is satisfied, and 0 otherwise. Selection of hyperparameters ϵ_1 and ϵ_2 can be performed by assessing quantiles of the empirical distribution of shape similarities and then cross-validation. Thresholds ϵ_1 and ϵ_2 are used to reinforce meaningful edge structures and suppress noisy edges.

How does TIMR help? TIMR allows us not only to inject a new edge among two nodes if shapes of their multi-hop neighborhoods are sufficiently close, but also to eliminate an existing edge if topological distance among their multi-hop node neighborhoods is higher than predefined threshold ϵ_2 . That is, TIMR adds an edge between the nodes whose “similarity” is detected by persistent homology, and removes the edge between “topologically dissimilar” nodes. This way, in the new TIMR graph, similar nodes gets closer, and dissimilar nodes gets farther away, thereby assisting throughout the node classification process. As a result, TIMR also mitigates the impact of noise edges and reduces the effect of over-fitting. Furthermore, while we have not formally explored TIMR in conjunction with formal defense mechanisms against adversarial attacks, TIMR may be viewed as an essential remedial ingredient in defense. Indeed, TIMR offers an insight about one of the key defense challenges [29], namely, systematic criteria we should follow to clean the attacked graph – TIMR suggests to recover edges removed by the attacker with positive topology-induced links and to suppress edges induced by the attacker with negative topology-induced links.

4.2 TIMR Theoretical Stability Guarantees

We now establish theoretical stability properties of the TIMR average degree. The average degree is known to be closely related to performance in node classification tasks [30, 19, 1] and, hence, degree-dependent regularization is often used in adversarial training [40, 53, 47]. Here we prove that under perturbations of the observed graph \mathcal{G} , average degrees of the TIMR graphs of the original and distorted copies remain close. That is, the proposed TRI framework allows us to increase robustness of the graph degree properties with respect to graph perturbations and attacks. Given that persistent homology representations are known to be robust against noise, our result appears to be intuitive. However, integration of graph persistent homology into node classification tasks and its theoretical guarantees remain yet an untapped area.

Let \mathcal{G}^+ and \mathcal{G}^- be two graphs of the same order. Let T^+ and T^- be TIMR graphs of \mathcal{G}^+ and \mathcal{G}^- , constructed by the degree based filtration. We define *local k -distance* between two graphs based on the Wasserstein distance d_{W_p} between their persistence diagrams as follows. Let u^\pm be a node in \mathcal{G}^\pm and $\mathcal{G}_{u^\pm}^k$ be k -neighborhood of the u^\pm in \mathcal{G}^\pm . Let

$$\mathbf{d}_k(u^+, u^-) = d_{W_1}(\mathcal{D}_0(\mathcal{G}_{u^+}^k), \mathcal{D}_0(\mathcal{G}_{u^-}^k)),$$

where d_{W_1} is Wasserstein-1 distance (see Definition 1), and $\mathcal{D}_0(\mathcal{G})$ is the persistence diagram of 0-cycles. Let $\varphi : V^+ \rightarrow V^-$ be a bijection between node sets of \mathcal{G}^+ and \mathcal{G}^- , respectively. Then, the local k -distance between \mathcal{G}^+ and \mathcal{G}^- is defined as

$$\mathfrak{D}^k(\mathcal{G}^+, \mathcal{G}^-) = \min_{\varphi} \sum_{u^+} \mathbf{d}_k(u^+, \varphi(u^+)).$$

We now have the following stability result:

Theorem 1 (Stability of Average Degree). Let \mathcal{G}^+ and \mathcal{G}^- be two graphs of same size and order. Let T^\pm be the TIMR graph induced by \mathcal{G}^\pm , with thresholds ϵ_1 and ϵ_2 . Let α^\pm be the average degree of T^\pm . Then, there exists a constant $K(\epsilon_1, \epsilon_2) > 0$ such that

$$|\alpha^+ - \alpha^-| \leq K(\epsilon_1, \epsilon_2) \mathfrak{D}^k(\mathcal{G}^+, \mathcal{G}^-).$$

The proof of the theorem is given in Appendix A in the supplementary material.

Furthermore, we conjecture the following result on stability of algebraic connectivity of TIMR graphs for the attribute based case. Here, the algebraic connectivity $\lambda_2(G)$ is the second smallest eigenvalue of the graph Laplacian $L(G)$, and it is considered to be a spectral measure to determine the robustness of the graph [48].

Conjecture: Let \mathcal{G} be a graph, and let \mathcal{G}' be a graph which is obtained by adding one edge e to \mathcal{G} , i.e., $\mathcal{G}' = \mathcal{G} \cup e$. Let T, T' be the TIMR graphs induced by $\mathcal{G}, \mathcal{G}'$, respectively. Then,

$$|\lambda_2(T') - \lambda_2(T)| \leq K(\epsilon_1, \epsilon_2) |\lambda_2(\mathcal{G}') - \lambda_2(\mathcal{G})|.$$

Note that this conjecture is not true for degree based TIMR graphs. The reason for that when one adds an edge e_{uv} to \mathcal{G} , then this operation significantly changes k -neighborhoods of all nodes in $N_k(v_i)$ and $N_k(v_j)$. Since degree based TIMR construction depends on persistence diagrams of these k -neighborhoods, adding such an edge causes an uncontrollable effect on the algebraic connectivity. However, in attribute based construction, similarity is only based on the attributes, and the distances in the graph does not have an effect on edge addition/deletion decision. So, when the original graph \mathcal{G} is perturbed by adding an edge, the attributes remain intact, and TIMR representations of the original and perturbed graphs are identical.

4.3 STAN: learning from Subgraphs, Topology and Attributes of Neighbors

For graphs with continuous or binary node features, higher-order form of message passing and aggregation (i.e., powers of the adjacency matrix) are shown to capture important structural graph properties that are inaccessible at the node-level. However, such higher-order architectures largely focus on global network topology and do not account for the important local graph structures. Also, performance of such higher-order graph convolution architectures tend to suffer from over-smoothing and be susceptible to noisy observations, since their propagation schemes recursively update each node's feature vector by aggregating over information delivered by all further nodes captured by a random walk.

Here we propose a new recursive feature propagation scheme **STAN** which updates the node features from **S**ubgraphs, **T**opology, and **A**tttributes of **N**eighbors. In particular, for each target node, STAN (i) converts these three features into a form of topological edge weights, (ii) calculates topological average of neighborhood features, (iii) aggregates them with the initial node features.

Let $X_u^{(0)} = X_u$ be the initial node features for $u \in \mathcal{V}$ and \mathcal{T} be the number of STAN iterations. Then we iteratively update the feature representation of node u using side information collected from nodes within its k -hop local neighborhood via $X_u^{(t+1)} = f_{\text{up}}\left(\phi_{\text{aggr}}\left(X_u^{(t)}, \alpha(u) \sum_{v \in \mathcal{V}_k(u)} \hat{d}_{uv} \cdot X_v^{(t)}\right)\right)$,

where f_{up} is the update function such as a *multi-layer perceptron (MLP)* and a *gated network*, ϕ_{aggr} is function that aggregates topological features into node features, such as *sum* and *mean*; $\alpha(u)$ is a weighting factor which can be set either as a hyperparameter or a fixed scalar, and \hat{d}_{uv} are normalized topological edge weights

$$\hat{d}_{uv} = \frac{\exp [(d_{W,p}^f(\mathcal{G}_u, \mathcal{G}_v))^{-1}]}{\sum_{v \in \mathcal{V}_k(u)} \exp [(d_{W,p}^f(\mathcal{G}_u, \mathcal{G}_v))^{-1}]}.$$

The core principle of STAN is to assign different importance scores to nodes, depending on how similar topologically their neighborhoods are to the target node, and to control the impact on the target node prediction when aggregating neighborhoods' information. For instance, suppose target node is u and we also have nodes v and w . We assign a higher weight to the edge between u and v (if the shapes of their neighborhoods are more similar) and a lower weight to the edge between u and w (if neighborhoods of u and w have more distinct topology). As a result, the updated node features of u will be more affected by v .

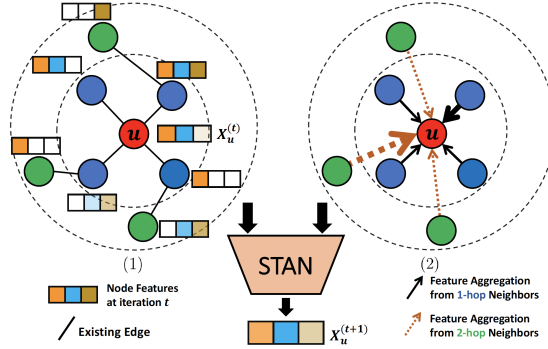


Figure 2: STAN for node feature vectors extension. The target node u (red) with 2-hop neighborhood, where four 1-hop neighbors (blue) and three 2-hop neighbors (green). Each node is represented by a 3-component feature vector. We include more discussion on the STAN in Appendix B.

4.4 Convolution based TRI-GNN Layer

We now turn to construction of the TRI-GNN layer. Let $\mathbf{W} \in \mathbb{R}^{N \times N \times 3}$ be a 3-dimension tensor, where N is the number of nodes and 3 is the number of candidate adjacency matrices (i.e., W , W^{topo^+} , and W^{topo^-}). Let W_{uvr} be the r -th type of edge between nodes u and v of \mathbf{W} , where $u \in \{1, \dots, N\}$, $v \in \{1, \dots, N\}$, and $r \in \{1, 2, 3\}$. That is, we denote W , W^{topo^+} , and W^{topo^-} by setting $r = 1, 2, 3$. We then consider a *joint topology-induced* adjacency matrix W^{topo}

$$W_{uv}^{\text{topo}} = \begin{cases} 1, & \text{if } \sum_r W_{uvr} > 0 \\ 0, & \text{otherwise} \end{cases}. \quad (3)$$

In the experiments, we utilize the classification function for the generalized semi-supervised learning as the default filter engine of TRI-GNN. Given W^{topo} , we compute topological distance-based graph Laplacian $L^{\text{topo}} = (\tilde{D}^{\text{topo}})^{-\sigma} \tilde{W}^{\text{topo}} (\tilde{D}^{\text{topo}})^{\sigma-1}$, where $\tilde{W}^{\text{topo}} = (W^{\text{topo}} + I)^\rho$, $\tilde{D}^{\text{topo}} = \sum_v \tilde{W}_{uv}^{\text{topo}}$, $\sigma \in [0, 1]$, and $\rho \in (0, \infty)$. Equipped with the new graph Laplacian L^{topo} and node information matrix $X^{(\mathcal{T})}$ at iteration \mathcal{T} , TRI-GNN uses the following graph convolution layer

$$H^{(\ell+1)} = \psi \left(\mu (I - \mu L^{\text{topo}})^{-1} H^{(\ell)} \Theta^{(\ell)} \right) = \psi \left(\mu \sum_{i=0}^{\infty} (\mu L^{\text{topo}})^i H^{(\ell)} \Theta^{(\ell)} \right),$$

where $\mu \in (0, 1]$ is a regularization parameter, $H^{(\ell)} \in \mathbb{R}^{N \times F_\ell}$ and $H^{(\ell+1)} \in \mathbb{R}^{N \times F_{\ell+1}}$ are input and output activations for layer ℓ ($H^{(0)} = X^{(\mathcal{T})}$), $\Theta \in \mathbb{R}^{F_\ell \times F_{\ell+1}}$ are the trainable parameters of TRI-GNN, and ψ is an element-wise nonlinear activation function such as ReLU. In the experiments μ is selected from $\{0.1, 0.2, \dots, 0.9\}$, and its choice impacts the number of terms in Taylor expansion. To reduce the computational complexity, based on the Taylor series expansion, we empirically find

that $\max_i = \lceil \mathcal{R}\mu \rceil$ is a suitable rule of thumb (where $\mathcal{R} \in [2, 50]$), while the closer σ is to 0, the more robust to the choice of regularization parameters the performance is. Note that in order to improve the robustness of TRI-GNN when it is exposed to noisy, we can consider convolution based TRI-GNN layer with parallel structure.

Table 1: Performance on semi-supervised classification. Average accuracy (%) and standard deviation (%) in ().

Method	IEEE 118-Bus	ACTIVSg200	ACTIVSg500	ACTIVSg2000	Cora-ML	CiteSeer	PubMed
ChebNet	60.00 (3.11)	80.63 (4.20)	95.18 (1.00)	80.04 (0.37)	81.45 (1.21)	70.23 (0.80)	78.40 (1.10)
GCN	52.86 (0.78)	82.96 (1.66)	90.33 (0.68)	73.36 (0.41)	81.50 (0.40)	71.11 (0.72)	79.00 (0.53)
MotifNet	65.75 (0.77)	73.20 (1.61)	95.18 (0.53)	82.00 (0.44)	-	-	-
ARMA	70.55 (2.23)	80.07 (3.30)	94.33 (0.47)	81.20 (0.23)	82.80 (0.63)	72.30 (0.44)	78.80 (0.30)
GAT	70.23 (1.80)	83.56 (2.58)	95.00 (0.47)	83.00 (0.59)	83.11 (0.70)	70.85 (0.70)	78.56 (0.31)
RGCN	81.80 (1.79)	83.35 (3.12)	95.91 (0.50)	85.23 (0.40)	82.80 (0.60)	72.13 (0.50)	79.11 (0.30)
GMNN	78.88 (2.50)	84.13 (1.89)	96.57 (0.52)	86.21 (0.29)	83.72 (0.90)	73.10 (0.79)	81.80 (0.53)
LGCNs	71.43 (2.20)	83.78 (1.50)	95.14 (0.45)	85.57 (0.25)	83.35 (0.51)	73.08 (0.63)	79.51 (0.22)
SPAGAN	78.55 (2.25)	81.83 (2.09)	96.19 (0.40)	86.00 (0.26)	83.63 (0.55)	73.02 (0.41)	79.60 (0.40)
APPNP	82.05 (2.24)	81.21 (1.85)	96.11 (0.45)	86.77 (0.30)	83.31 (0.53)	72.30 (0.51)	80.12 (0.20)
VPN	82.19 (2.20)	79.89 (1.82)	96.23 (0.50)	86.87 (0.33)	81.89 (0.57)	71.40 (0.32)	79.60 (0.39)
LFGCN	82.20 (2.30)	81.11 (2.10)	97.61 (0.47)	87.74 (0.30)	84.35 (0.57)	71.89 (0.77)	79.60 (0.55)
MixHop	80.05 (2.50)	80.53 (1.96)	95.94 (0.40)	86.10 (0.25)	81.90 (0.81)	71.41 (0.40)	80.81 (0.58)
PEGN-RC	82.30 (1.90)	83.30 (1.10)	97.20 (0.50)	87.62 (0.74)	82.70 (0.50)	71.91 (0.63)	79.40 (0.70)
TRI-GNN _A	82.80 (1.64)	84.93 (1.51)	97.85 (0.56)	88.82 (0.56)	84.80 (0.55)	73.45 (0.65)	79.80 (0.52)
TRI-GNN _D	82.67 (2.08)	86.18 (0.20)	98.11 (0.43)	89.06 (0.44)	84.98 (0.49)	73.32 (0.48)	79.70 (0.50)

5 Experiments

We now empirically evaluate the effectiveness of our proposed method on seven node-classification benchmarks under semi-supervised setting with different graph size and feature type. We run all experiments for 50 times and report the average accuracy results and standard deviations.

5.1 Experimental Settings

Datasets We compare TRI-GNN with the state-of-the-art (SOA) baselines, using standard publicly available real and synthetic networks: (1) 3 citation networks [44]: Cora-ML, CiteSeer, and PubMed, where nodes are publications and edges are citations; (2) 4 synthetic power grid networks [8, 7, 25]: IEEE 118-bus system, ACTIVSg200 system, ACTIVSg500 system, and ACTIVSg2000 system, where each node represents a load bus, transformer, or generator and we use total line charging susceptance (BR_B) as edge weight. For more details see Table 3 (in Appendix C.1).

Baselines We compare TRI-GNN with 14 SOA GNNs: (i) 5 higher-order graph convolution architectures: LGCNs [24], APPNP [33], VPN [27], LFGCN [15], and MixHop [3]; (ii) 2 graph attention mechanism: GAT [51] and SPAGAN [57]; (iii) 4 GNNs with polynomial filters: ChebNet [20], GCN [32], MotifNet [37], and ARMA [6]; (iv) 2 GNNs by learning the generative distribution: GMNN [41] and RGCN [62]; and (v) 1 GNNs with topological information: PEGN-RC [61]. In the experiments, we implement two variants of TRI-GNN, i.e., TRI-GNN_A (node attributes as filtration function) and TRI-GNN_D (node degree as filtration function). In addition, in our robustness experiments, we select the 4 strongest baselines in each of the GNN areas: random walks, graph attention networks, higher-order graph convolutional models, and robust graph convolutional networks (i.e., APPNP, GAT, LFGCN, and RGCN). More details on experimental setup are in Appendix C.2. The source code of TRI-GNN is publicly available at <https://github.com/TRI-GNN/TRI-GNN.git>.

5.2 Performance on Node Classification

Table 1 shows the results for node classification results on graphs. We observe that TRI-GNN outperforms all baselines on CoraML, CiteSeer, and four power grid networks, while achieving comparable performance on PubMed. This consistently strong performance of TRI-GNN indicates utility of integrating more complex graph structures through aggregating higher-order topological information. The best results are highlighted in bold for all datasets. As Table 1 shows, TRI-GNN_D and TRI-GNN_A outperform all baselines on all 7 but 1 benchmark datasets, yielding relative gains of 0.5-2.5% on clean graphs. Overall, TRI-GNN_D appears to be the most competitive approach,

especially for ACTIVSg200 and ACTIVSg500 systems. Nevertheless, TRI-GNN_A tends to follow TRI-GNN_D relatively closely. It validates that the framework of topological relational inference can integrate topological information across multigraph representation and feature propagation, respectively. On PubMed, GMNN achieves a better accuracy than both TRI-GNN versions due to PubMed exhibiting the weakest structural information with very few links per node on average, but both TRI-GNN models still deliver highly competitive results. In addition, we find that for sparser heterogeneous graphs, with lower numbers of node attributes per class, richer topological structure (i.e., synthetic ACTIVSg200 and ACTIVSg2000) and weaker dependency between attributes and classes, PH induced by the graph properties is more important than attribute-induced PH, while for denser, more homogeneous graphs as IEEE 118-bus, attribute-based filtration is the key. These insights echo findings in real citation networks.

Ablation Study Our TRI framework contains two key components: (i) encoding higher-order topological information via TIMR, (ii) STAN, i.e., updating the node features by aggregating information from subgraphs, topology, and neighborhood features. To glean a deeper insight into how different components help TRI-GNN to achieve highly competitive results, we conduct experiments by removing individual component separately, namely (1) TRI-GNN_D w/o TIMR (i.e., denoted by Ω), (2) TRI-GNN_D w/o STAN, and (3) TRI-GNN_D with TIMR and STN (where STN represents updating the node features by only aggregating information from subgraphs and topology without neighborhood features). As Table 2 shows, both TIMR Ω and STAN indeed yield significant performance improvements on all datasets. The ablation study on contribution of TIMR and STAN with TRI-GNN_A are in Table 5 of Appendix C.3. The results show that all the components are indispensable.

Table 2: TRI-GNN_D ablation study. Significance analysis is performed with one-sided two-sample t -test based on 50 runs; *, **, *** denote p -value < 0.1, 0.05, 0.01 (i.e., significant, statistically significant, highly statistically significant).

Dataset	TRI-GNN _D	w/o Ω	w/o STAN	with Ω , STN
ACTIVSg200	86.18 (0.20)	***82.93 (1.32)	***83.00 (3.17)	***83.25 (1.58)
ACTIVSg500	98.11 (0.43)	***93.71 (1.03)	***94.31 (1.20)	***93.69 (1.50)
Cora-ML	84.98 (0.49)	***84.26 (0.77)	***84.00 (0.33)	***84.40 (0.56)
CiteSeer	73.32 (0.48)	**73.11 (0.43)	73.20 (0.55)	*73.19 (0.47)

Boundary Sensitivity We select the ϵ_1 and ϵ_2 values based on quantiles of Wasserstein distances between persistence diagrams (see Figure 3a). The optimal choice of ϵ_1 and ϵ_2 can be obtained via cross-validation. For instance, the optimal quantile of ϵ_1 and ϵ_2 for ACTIVSg200 dataset is 0.55 and 2.50 respectively. We consider the lower and upper bounds for ϵ_1 are 0.50 (minimum) and 0.05-quantile, respectively, and the lower and upper bounds for ϵ_2 are 0.1-quantile and 6.74 (maximum), respectively. For ϵ_1 , we generate a sequence from 0.50 to 2.00 with increment of the sequence 0.05; for ϵ_2 , we generate a sequence from 2.50 to 6.74 with increment of the sequence 0.5. Based on cross-validation, we conduct experiments in different ϵ_1 and ϵ_2 combinations. Figures 3b and 3c show the performances with respect to different thresholds (ϵ_1 and ϵ_2) combinations (where \dagger denotes the ϵ_i (where $i \in \{1, 2\}$) is not fixed). From the results in Figure 3, we find that (ϵ_1, ϵ_2) around (0.55, 2.50) tend to deliver the optimal performance (accuracy (%)). The optimal results differ among graphs and depend on sparsity, label rates and graph higher-order properties. To better examine the boundary sensitivity, we further evaluate hyperparameters ϵ_1 and ϵ_2 on ACTIVSg500 in Appendix C.8.

Robustness Analysis To evaluate the model performance under graph perturbations, we test the robustness of the TRI-GNN framework under random attacks (here we present the results for TRI-GNN_A, and analogous robustness for TRI-GNN_D are in Appendix C.4.). Random attack randomly generates fake edges and injects them into the existing graph structure. The ratio of the number of fake edges to the number of existing edges varies from 0 to 100%. As Figure 4 shows, TRI-GNN_A consistently outperforms all baselines on both citation and power grid networks under random attacks, delivering gains up to 10% in highly noisy scenarios (see Cora-ML). These findings indicate that TRI-GNN_A is again the most robust GNN node classifier under random attacks. By aggregating local topological information from node features and neighborhood substructures, TRI-GNN_A can “absorb” noisy edges and, as a result, exhibits less sensitivity to graph perturbations and adversarial attacks.

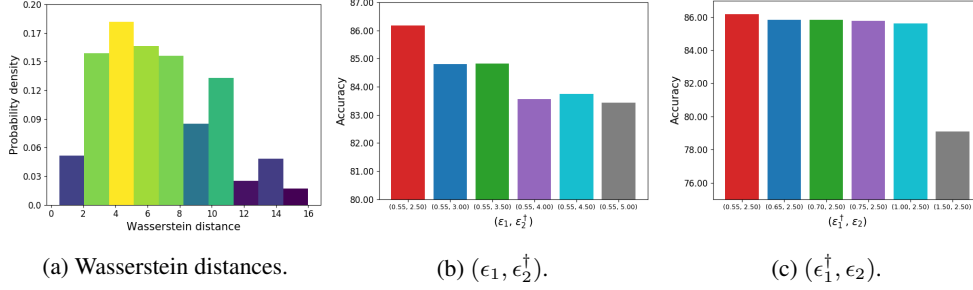


Figure 3: Hyperparameters ϵ_1 and ϵ_2 selection of TRI-GNN on ACTIVSg200 dataset.

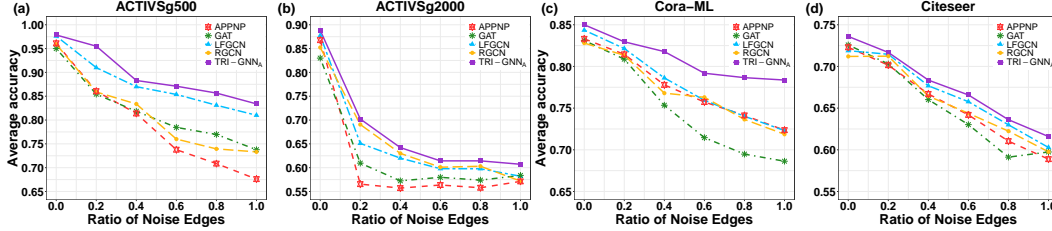


Figure 4: Node classification accuracy under random attacks.

Computational Costs In less extreme scenarios, the expected number of nodes in the k -hop neighborhood can be approximated by \bar{d}^k , where \bar{d} is the mean degree of the graph and mathematical expectation is in terms of the node degree distribution. The computational complexity for Wasserstein distance between two persistence diagrams is $\mathcal{O}(M^3)$, where M is the total number of barcodes in the both persistence diagrams. In the worst case scenario, if we use a very fine filtering function for persistence diagrams of k -hop neighborhoods, it would give at most $2\bar{d}^k$ barcodes (i.e., the number of barcodes in each k -hop neighborhood is at most \bar{d}^k and we compare two k -hop neighborhoods). Considering we use the degree filtering function for our persistence diagrams, we expect to have much less ($\sim \bar{d}^k$) barcodes in the 0-th persistence diagram of a k -hop neighborhood by using the technique in [31]. Hence, the overall computational complexity would be of stochastic order $\mathcal{O}(N^2 \bar{d}^{\frac{3k}{2}})$. It may be costly to run PH for denser graphs (currently, computational complexity is the main roadblock for all PH-based methods on graphs) but as we noted earlier, for denser graphs we may use a degree filtration under lower k -hops which is still found to be very powerful even for small k . Table 4 in Appendix C.2 reports the average running time of PD generation and training time per epoch of our TRI-GNN model on all datasets.

6 Conclusion

We have proposed a novel perspective to node classification with GNN, based on the TDA concepts invoked within each local node neighborhood. The new TRI approach has shown to deliver highly competitive results on clean graphs and substantial improvements in robustness against graph perturbations. In the future, we plan to apply TRI-GNN as a part of structured graph pooling.

Societal Impact and Limitations

Among the major limitations we currently see is probable existence of the bias of the proposed node classification approach due to potentially unbalanced population groups [5]. Indeed, in the context of social data analysis, given that we analyze peer neighborhoods which themselves tend to be largely formed by the same users as the target node and hence are likely to be dominated by the abundant group, such bias is very likely to exist and to be non-negligible. Mitigating it is a problem on its own but some ideas include using multiple filtration functions based on different node attributes so the node neighborhoods are made more diverse and are no longer dominated by a specific group or removing some potentially sensitive node attributes (e.g., gender) completely from the study (which has its own pros and cons in terms of accuracy).

Acknowledgements

This material is based upon work sponsored by the National Science Foundation under award numbers ECCS 2039701, INTERN supplement for ECCS 1824716, DMS 1925346 and the Department of the Navy, Office of Naval Research under ONR award number N000142112226. Any opinions, findings, and conclusions or recommendations expressed in this material are those of the author(s) and do not necessarily reflect the views of the Office of Naval Research. The authors are also grateful to the NeurIPS anonymous reviewers for many insightful suggestions and engaging discussion which improved clarity of the manuscript and highlighted new open research directions.

References

- [1] Emmanuel Abbe, Enric Boix-Adsera, Peter Ralli, and Colin Sandon. Graph powering and spectral robustness. *SIAM Journal on Mathematics of Data Science*, 2(1):132–157, 2020.
- [2] Sami Abu-El-Haija, Amol Kapoor, Bryan Perozzi, and Joonseok Lee. N-GCN: Multi-scale graph convolution for semi-supervised node classification. In *UAI*, pages 841–851, 2020.
- [3] Sami Abu-El-Haija, Bryan Perozzi, Amol Kapoor, Nazanin Alipourfard, Kristina Lerman, Hrayr Harutyunyan, Greg Ver Steeg, and Aram Galstyan. Mixhop: Higher-order graph convolutional architectures via sparsified neighborhood mixing. In *ICML*, pages 21–29, 2019.
- [4] Konstantin Avrachenkov and Maximilien Dreveton. Almost exact recovery in noisy semi-supervised learning. *arXiv:2007.14717*, 2020.
- [5] Solon Barocas, Moritz Hardt, and Arvind Narayanan. *Fairness and Machine Learning*. fairmlbook.org, 2021. <http://www.fairmlbook.org>.
- [6] Filippo Maria Bianchi, Daniele Grattarola, Lorenzo Livi, and Cesare Alippi. Graph neural networks with convolutional arma filters. *TPAMI*, 2021.
- [7] Adam B Birchfield, Kathleen M Gegner, Ti Xu, Komal S Shetye, and Thomas J Overbye. Statistical considerations in the creation of realistic synthetic power grids for geomagnetic disturbance studies. *Transactions on Power Systems*, 32(2):1502–1510, 2016.
- [8] Adam B Birchfield, Ti Xu, Kathleen M Gegner, Komal S Shetye, and Thomas J Overbye. Grid structural characteristics as validation criteria for synthetic networks. *Transactions on Power Systems*, 32(4):3258–3265, 2016.
- [9] Michael M Bronstein, Joan Bruna, Yann LeCun, Arthur Szlam, and Pierre Vandergheynst. Geometric deep learning: going beyond euclidean data. *Signal Processing Magazine*, 34(4):18–42, 2017.
- [10] Joan Bruna, Wojciech Zaremba, Arthur Szlam, and Yann LeCun. Spectral networks and locally connected networks on graphs. In *ICLR*, 2014.
- [11] Gunnar Carlsson. Topological pattern recognition for point cloud data. *Acta Numerica*, 23:289–368, 2014.
- [12] Mathieu Carrière, Frédéric Chazal, Yuichi Ike, Théo Lacombe, Martin Royer, and Yuhei Umeda. Perslay: A neural network layer for persistence diagrams and new graph topological signatures. In *AISTATS*, pages 2786–2796, 2020.
- [13] Frédéric Chazal and Bertrand Michel. An introduction to topological data analysis: fundamental and practical aspects for data scientists. *Frontiers in Artificial Intelligence*, 4, 2021.
- [14] Deli Chen, Yankai Lin, Wei Li, Peng Li, Jie Zhou, and Xu Sun. Measuring and relieving the over-smoothing problem for graph neural networks from the topological view. In *AAAI*, pages 3438–3445, 2020.
- [15] Yuzhou Chen, Yulia R Gel, and Konstantin Avrachenkov. LFGCN: Levitating over graphs with levy flights. In *ICDM*, pages 960–965. IEEE, 2020.
- [16] Yuzhou Chen, Yulia R Gel, Vyacheslav Lyubchich, and Todd Winship. Deep ensemble classifiers and peer effects analysis for churn forecasting in retail banking. In *PaKDD*, pages 373–385, 2018.
- [17] Zhiqian Chen, Fanglan Chen, Lei Zhang, Taoran Ji, Kaiqun Fu, Liang Zhao, Feng Chen, and Chang-Tien Lu. Bridging the gap between spatial and spectral domains: A survey on graph neural networks. *arXiv:2002.11867*, 2020.

- [18] Shrey Dabhi and Manojkumar Parmar. NodeNet: A graph regularised neural network for node classification. *arXiv preprint arXiv:2006.09022*, 2020.
- [19] Hanjun Dai, Hui Li, Tian Tian, Xin Huang, Lin Wang, Jun Zhu, and Le Song. Adversarial attack on graph structured data. In *ICML*, pages 1115–1124, 2018.
- [20] Michaël Defferrard, Xavier Bresson, and Pierre Vandergheynst. Convolutional neural networks on graphs with fast localized spectral filtering. In *NeurIPS*, pages 3844–3852, 2016.
- [21] Tyler Derr, Yao Ma, Wenqi Fan, Xiaorui Liu, Charu Aggarwal, and Jiliang Tang. Epidemic graph convolutional network. In *WSDM*, pages 160–168, 2020.
- [22] Michel Marie Deza and Elena Deza. Encyclopedia of distances. In *Encyclopedia of Distances*, pages 1–583. Springer, 2009.
- [23] Herbert Edelsbrunner and John Harer. *Computational topology: an introduction*. American Mathematical Soc., 2010.
- [24] Hongyang Gao, Zhengyang Wang, and Shuiwang Ji. Large-scale learnable graph convolutional networks. In *ACM SIGKDD*, pages 1416–1424, 2018.
- [25] Kathleen M Gegner, Adam B Birchfield, Ti Xu, Komal S Shetye, and Thomas J Overbye. A methodology for the creation of geographically realistic synthetic power flow models. In *PECI*, pages 1–6. IEEE, 2016.
- [26] Christoph D Hofer, Roland Kwitt, and Marc Niethammer. Learning representations of persistence barcodes. *JMLR*, 20(126):1–45, 2019.
- [27] Ming Jin, Heng Chang, Wenwu Zhu, and Somayeh Sojoudi. Power up! robust graph convolutional network via graph powering. In *AAAI*, 2021.
- [28] Wei Jin, Yaxing Li, Han Xu, Yiqi Wang, Shuiwang Ji, Charu Aggarwal, and Jiliang Tang. Adversarial attacks and defenses on graphs: A review, a tool and empirical studies. *ACM SIGKDD Explorations Newsletter*, page 19–34, 2021.
- [29] Wei Jin, Yao Ma, Xiaorui Liu, Xianfeng Tang, Suhang Wang, and Jiliang Tang. Graph structure learning for robust graph neural networks. In *ACM SIGKDD*, 2020.
- [30] Antony Joseph and Bin Yu. Impact of regularization on spectral clustering. *The Annals of Statistics*, 44(4):1765–1791, 2016.
- [31] Lida Kanari, Adélie Garin, and Kathryn Hess. From trees to barcodes and back again: theoretical and statistical perspectives. *Algorithms*, 13(12):335, 2020.
- [32] Thomas N Kipf and Max Welling. Semi-supervised classification with graph convolutional networks. In *ICLR*, 2017.
- [33] Johannes Klicpera, Aleksandar Bojchevski, and Stephan Günnemann. Predict then propagate: Graph neural networks meet personalized pagerank. In *ICLR*, 2019.
- [34] Panagiotis Kyriakis, Iordanis Fostirooulos, and Paul Bogdan. Learning hyperbolic representations of topological features. In *ICLR*, 2021.
- [35] Tam Le and Makoto Yamada. Persistence fisher kernel: A riemannian manifold kernel for persistence diagrams. In *NeurIPS*, pages 10007–10018, 2018.
- [36] Meng Liu, Hongyang Gao, and Shuiwang Ji. Towards deeper graph neural networks. In *ACM SIGKDD*, pages 338–348, 2020.
- [37] Federico Monti, Karl Otness, and Michael M Bronstein. Motifnet: a motif-based graph convolutional network for directed graphs. In *DSW*, pages 225–228. IEEE, 2018.
- [38] Elchanan Mossel and Jiaming Xu. Local algorithms for block models with side information. In *ITCS*, pages 71–80, 2016.
- [39] Elizabeth Munch. A user’s guide to topological data analysis. *Journal of Learning Analytics*, 4(2):47–61, 2017.
- [40] Sharad Nandanwar and M Narasimha Murty. Structural neighborhood based classification of nodes in a network. In *ACM SIGKDD*, pages 1085–1094, 2016.

- [41] Meng Qu, Yoshua Bengio, and Jian Tang. GMNN: Graph markov neural networks. In *ICML*, pages 5241–5250, 2019.
- [42] Bastian Rieck, Christian Bock, and Karsten Borgwardt. A persistent weisfeiler-lehman procedure for graph classification. In *ICML*, pages 5448–5458, 2019.
- [43] Yu Rong, Wenbing Huang, Tingyang Xu, and Junzhou Huang. Dropedge: Towards deep graph convolutional networks on node classification. In *ICLR*, 2019.
- [44] Prithviraj Sen, Galileo Namata, Mustafa Bilgic, Lise Getoor, Brian Galligher, and Tina Eliassi-Rad. Collective classification in network data. *AI Magazine*, 29(3):93–93, 2008.
- [45] Ke Sun, Piotr Koniusz, and Zhen Wang. Fisher-bures adversary graph convolutional networks. In *UAI*, pages 465–475. PMLR, 2020.
- [46] Lichao Sun, Yingtong Dou, Carl Yang, Ji Wang, Philip S Yu, and Bo Li. Adversarial attack and defense on graph data: A survey. *arXiv:1812.10528*, 2020.
- [47] Yiwei Sun, Suhang Wang, Xianfeng Tang, Tsung-Yu Hsieh, and Vasant Honavar. Non-target-specific node injection attacks on graph neural networks: A hierarchical reinforcement learning approach. In *WWW*, volume 3, 2020.
- [48] Ali Sydney, Caterina Scoglio, and Don Gruenbacher. Optimizing algebraic connectivity by edge rewiring. *Applied Mathematics and Computation*, 219(10):5465–5479, 2013.
- [49] Matteo Toginalli, Elisabetta Ghisu, Felipe Llinares-López, Bastian Rieck, and Karsten Borgwardt. Wasserstein weisfeiler-lehman graph kernels. In *NeurIPS*, pages 6439–6449, 2019.
- [50] Francesco Tudisco, Austin R Benson, and Konstantin Prokopychik. Nonlinear higher-order label spreading. In *WWW*, pages 2402–2413, 2021.
- [51] P. Veličković, G. Cucurull, A. Casanova, A. Romero, P. Lio, and Y. Bengio. Graph attention networks. In *ICLR*, 2018.
- [52] Hongwei Wang and Jure Leskovec. Unifying graph convolutional neural networks and label propagation. *arXiv preprint arXiv:2002.06755*, 2020.
- [53] Shen Wang, Zhengzhang Chen, Jingchao Ni, Xiao Yu, Zhichun Li, Haifeng Chen, and Philip S Yu. Adversarial defense framework for graph neural network. *arXiv:1905.03679*, 2019.
- [54] Asiri Wijesinghe and Qing Wang. DFNets: Spectral cnns for graphs with feedback-looped filters. In *NeurIPS*, pages 6009–6020, 2019.
- [55] Huijun Wu, Chen Wang, Yuriy Tyshetskiy, Andrew Docherty, Kai Lu, and Liming Zhu. Adversarial examples on graph data: Deep insights into attack and defense. In *IJCAI*, 2019.
- [56] Zonghan Wu, Shirui Pan, Fengwen Chen, Guodong Long, Chengqi Zhang, and S Yu Philip. A comprehensive survey on graph neural networks. *TNNLS*, 2020.
- [57] Yiding Yang, Xinchao Wang, Mingli Song, Junsong Yuan, and Dacheng Tao. SPAGAN: shortest path graph attention network. In *IJCAI*, pages 4099–4105, 2019.
- [58] Monisha Yuvaraj, Asim K Dey, Vyacheslav Lyubchich, Yulia R Gel, and H Vincent Poor. Topological clustering of multilayer networks. *Proceedings of the National Academy of Sciences*, 118(21), 2021.
- [59] Ziwei Zhang, Peng Cui, and Wenwu Zhu. Deep learning on graphs: A survey. *TKDE*, 2020.
- [60] Qi Zhao and Yusu Wang. Learning metrics for persistence-based summaries and applications for graph classification. In *NeurIPS*, pages 9859–9870, 2019.
- [61] Qi Zhao, Ze Ye, Chao Chen, and Yusu Wang. Persistence enhanced graph neural network. In *AISTATS*, pages 2896–2906. PMLR, 2020.
- [62] Dingyuan Zhu, Ziwei Zhang, Peng Cui, and Wenwu Zhu. Robust graph convolutional networks against adversarial attacks. In *ACM SIGKDD*, pages 1399–1407, 2019.
- [63] Afra Zomorodian and Gunnar Carlsson. Computing persistent homology. *Discrete & Computational Geometry*, 33(2):249–274, 2005.

Checklist

1. For all authors...
 - (a) Do the main claims made in the abstract and introduction accurately reflect the paper's contributions and scope? [Yes]
 - (b) Did you describe the limitations of your work? [Yes] See Section 5.2, scalability.
 - (c) Did you discuss any potential negative societal impacts of your work? [N/A]
 - (d) Have you read the ethics review guidelines and ensured that your paper conforms to them? [Yes]
2. If you are including theoretical results...
 - (a) Did you state the full set of assumptions of all theoretical results? [Yes] See Section 4.2.
 - (b) Did you include complete proofs of all theoretical results? [Yes] See Supplementary Material, Appendix A.
3. If you ran experiments...
 - (a) Did you include the code, data, and instructions needed to reproduce the main experimental results (either in the supplemental material or as a URL)? [Yes] See Section 5 and Appendix C. Source code and data are publicly available at <https://github.com/TRI-GNN/TRI-GNN.git>.
 - (b) Did you specify all the training details (e.g., data splits, hyperparameters, how they were chosen)? [Yes] See Section 5 and Appendix C.
 - (c) Did you report error bars (e.g., with respect to the random seed after running experiments multiple times)? [Yes] See Section 5 and results on statistical hypothesis testing.
 - (d) Did you include the total amount of compute and the type of resources used (e.g., type of GPUs, internal cluster, or cloud provider)? [Yes] See Section 5 and Appendix C.
4. If you are using existing assets (e.g., code, data, models) or curating/releasing new assets...
 - (a) If your work uses existing assets, did you cite the creators? [Yes]
 - (b) Did you mention the license of the assets? [Yes]
 - (c) Did you include any new assets either in the supplemental material or as a URL? [Yes]
 - (d) Did you discuss whether and how consent was obtained from people whose data you're using/curating? [Yes]
 - (e) Did you discuss whether the data you are using/curating contains personally identifiable information or offensive content? [N/A]
5. If you used crowdsourcing or conducted research with human subjects...
 - (a) Did you include the full text of instructions given to participants and screenshots, if applicable? [N/A]
 - (b) Did you describe any potential participant risks, with links to Institutional Review Board (IRB) approvals, if applicable? [N/A]
 - (c) Did you include the estimated hourly wage paid to participants and the total amount spent on participant compensation? [N/A]

A Proof of Stability of Average Degree

In this part, we prove the following stability result. We use the notation from the paper.

Theorem 2 (Stability of Average Degree). Let \mathcal{G}^+ and \mathcal{G}^- be two graphs of same size and order. Let T^\pm be the TIMR graph induced by \mathcal{G}^\pm , with thresholds ϵ_1 and ϵ_2 . Let α^\pm be the average degree of T^\pm . Then, there exists a constant $K(\epsilon_1, \epsilon_2) > 0$ such that

$$|\alpha^+ - \alpha^-| \leq K(\epsilon_1, \epsilon_2) \mathfrak{D}^k(\mathcal{G}^+, \mathcal{G}^-).$$

Proof. For simplicity, we assume only that we add edges to \mathcal{G}^\pm to obtain T^\pm . The case for removing edges is similar. As \mathcal{G}^+ and \mathcal{G}^- are of the same order, number of nodes $V(\mathcal{G}^\pm) = V(T^\pm)$, say m . Let $E(\mathcal{G})$ represents the number of edges in the graph \mathcal{G} . Assume we added k^\pm edges to \mathcal{G}^\pm and get T^\pm , i.e. $E(T^\pm) - E(\mathcal{G}^\pm) = k^\pm$. Recall that average degree of a graph $\alpha(\mathcal{G}) = 2E(\mathcal{G})/V(\mathcal{G})$. Hence,

$$\begin{aligned} \alpha^+ = \alpha(T^+) &= \frac{2E(T^+)}{m} = \frac{2(E(\mathcal{G}^+) + k^+)}{m} \\ &= \alpha(\mathcal{G}^+) + \frac{2k^+}{m}. \end{aligned}$$

Similarly, $\alpha^- = \alpha(T^-) = \alpha(\mathcal{G}^-) + \frac{2k^-}{m}$. As \mathcal{G}^+ and \mathcal{G}^- are of the same size,

$$|\alpha^+ - \alpha^-| = \left| \frac{2k^+}{m} - \frac{2k^-}{m} \right| = \frac{2}{m} |k^+ - k^-|.$$

If we can bound this quantity in terms of $\mathfrak{D}^k(\mathcal{G}^+, \mathcal{G}^-)$, then the result follows. Notice that adding k^+ edges to \mathcal{G}^+ implies that there exist k^+ pairs of nodes $\{(u_1^+, v_1^+), (u_2^+, v_2^+), \dots, (u_{k^+}^+, v_{k^+}^+)\}$ in \mathcal{G}^+ such that $\mathbf{d}_k(u_i^+, v_i^+) < \epsilon_1$. We claim that we can find suitable $K(\epsilon_1) > 0$ such that $k^+ \sim k^-$ delivering the desired inequality.

Assume $\mathfrak{D}^k(\mathcal{G}^+, \mathcal{G}^-) = \delta$ where $\delta > 0$. Let $\varphi : \mathcal{G}^+ \rightarrow \mathcal{G}^-$ be the best matching for this metric. Notice that

$$\mathbf{d}_k(\varphi(u^+), \varphi(v^+)) \leq \mathbf{d}_k(\varphi(u^+), u^+) + \mathbf{d}_k(u^+, v^+) + \mathbf{d}_k(v^+, \varphi(v^+))$$

By assumption,

$$\begin{aligned} \mathbf{d}_k(u^+, \varphi(u^+)) &\leq \mathfrak{D}^k(\mathcal{G}^+, \mathcal{G}^-) = \delta \\ \mathbf{d}_k(v^+, \varphi(v^+)) &\leq \mathfrak{D}^k(\mathcal{G}^+, \mathcal{G}^-) = \delta, \end{aligned}$$

which implies

$$\mathbf{d}_k(\varphi(u^+), \varphi(v^+)) \leq 2\delta + \epsilon_1. \quad (4)$$

Let $k^+(t)$ be the number of pairs of points in \mathcal{G}^+ with PD distance $< t$, and define $k^-(t)$ likewise. We compare these two functions with respect to δ , PD distance of \mathcal{G}^+ and \mathcal{G}^- . Notice that both functions are monotone nondecreasing, and since there are only finitely many values, they are both locally constant. As $\varphi(u^+), \varphi(v^+)$ are both nodes in \mathcal{G}^- , the inequality (4) shows $k^+(t) < k^-(2\delta + t)$, i.e., for each pair $u^+, v^+ \in \mathcal{G}^+$ with k -neighborhoods of u^+ and v^+ are t -close, we will have the pair $\varphi(u^+), \varphi(v^+) \in \mathcal{G}^-$ whose k -neighborhoods are $(2\delta + t)$ -close. Similarly, we have $k^-(t) < k^+(2\delta + t)$. By taking $t = s - 2\delta$, we have $k^+(s - 2\delta) < k^-(s)$. Hence, assuming $k^+(t) > k^-(t)$ at t , this implies $k^+(t) - k^-(t) < k^+(t) - k^+(t - 2\delta)$. Hence, bounding $\frac{k^+(t) - k^+(t - 2\delta)}{\delta}$ by a constant $K(t)$ would suffice to finish the proof as δ is the PD distance appearing in the right hand side of the desired inequality.

Now, let r_0 be the minimum distance between the threshold pairs $\{(b, d)\}$ on the persistence diagram grid. Then, $d_k(u, v) \geq r_0$ for any $u, v \in \mathcal{G}^\pm$. Let $M = m \cdot (m - 1)/2$ be the total number of pairs in \mathcal{G}^\pm , i.e. $k^\pm \leq M$. Let $K_0 = 2M/r_0$. Now note that if $2\delta < r_0$, $k^+(t) - k^-(t - 2\delta) = 0$ for any threshold t , as by assumption, both k^\pm are locally constant for intervals of at least r_0 length. If $2\delta \geq r_0$, then $K_0 \cdot \delta \geq M$. As a result, since $k^+(t) - k^-(t) \leq M$ as M is the total number of pairs in \mathcal{G}^\pm , the proof follows. \square

B More detailed information of TRI-GNN

Figure 5 provides the overview of framework of TRI-GNN. For Figure 6, we provide more detailed descriptions of STAN within the Figure caption.

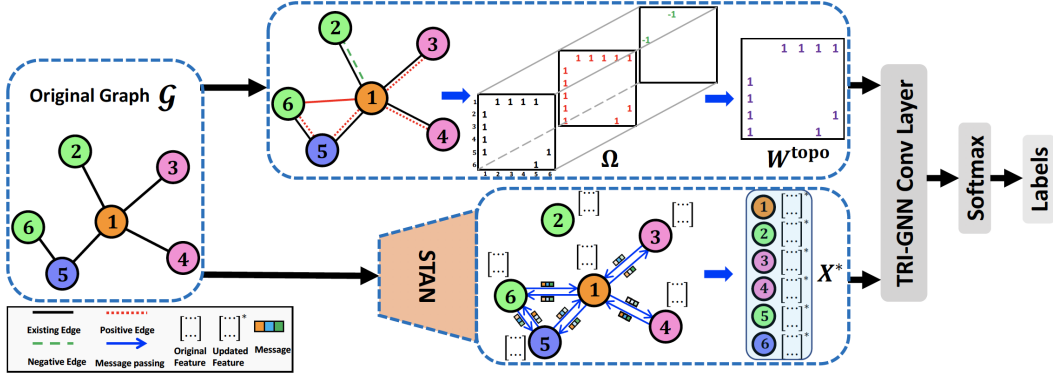


Figure 5: The framework of semi-supervised learning with TRI-GNN. Given the original graph \mathcal{G} , the upper part is the model architecture using topology-induced multigraph representation (Ω) equipped with a set of multiedges (see Eq. (1) in Definition 3 of the main manuscript) to obtain the *joint topology-induced* adjacency matrix W^{topo} . Here **edge colored black** represents the original edge in the graph \mathcal{G} (i.e., W), **edge colored red** represents *positive topology-induced* edge (i.e., W^{topo^+}), and **edge colored green** represents *negative topology-induced* edge (i.e., W^{topo^-}). The lower part is the model architecture using STAN to update node feature vectors (i.e., X^*) through weighted feature aggregation procedure based on topological distances. We then apply TRI-GNN convolutional layer and use the *joint topology-induced* adjacency matrix W^{topo} and updated node feature vectors X^* as input.

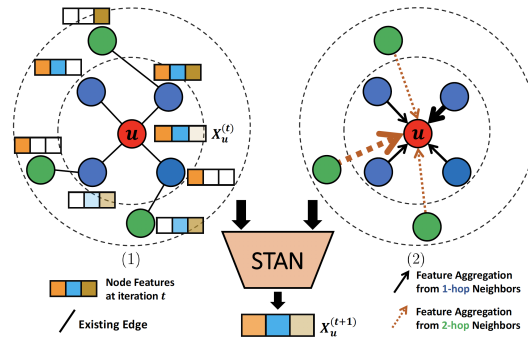


Figure 6: STAN for node feature vectors extension. The target node u (red) with 2-hop neighborhood, where four 1-hop neighbors (blue) and three 2-hop neighbors (green). Each node is represented by a 3-component feature vector. STAN utilizes node features from 2-hop neighborhood and normalized reciprocal topological distances (i.e., \hat{d}_{uv}) between the target node and its 2-hop neighborhood to produce a new vector representation for u . (1) shows node feature vectors for all nodes in 2-hop neighborhood of u at iteration t . (2) shows normalized reciprocal topological distances (which can be treated as edge weights) between 2-hop neighborhood and u , solid arrow indicates the weights during 1-hop neighborhood feature aggregation and dashed arrow indicates the weights during 2-hop neighborhood feature aggregation. After one iteration, STAN is applied to generate the feature vector for u at iteration $t+1$.

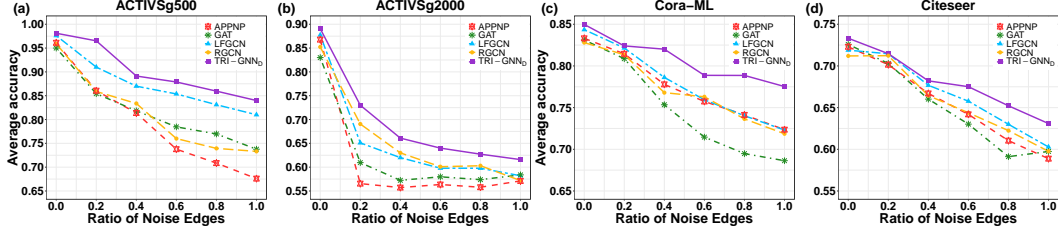


Figure 7: Node classification accuracy of TRI-GNN_D under random attacks.

Table 3: Dataset summary statistics.

Dataset	Vertices	Edges	Features	Classes	Label rate
IEEE 118-Bus	118	175	2	3	0.100
ACTIVSg200	200	156	5	3	0.100
ACTIVSg500	500	292	5	3	0.100
ACTIVSg2000	2,000	1,917	5	3	0.100
Cora-ML	2,708	5,429	1,433	7	0.052
CiteSeer	3,327	4,732	3,703	6	0.036
PubMed	19,717	44,338	500	3	0.003

C More details on experiments

C.1 Datasets

Undirected networks Cora-ML (this Cora dataset consists of Machine Learning papers), Citeseer and PubMed are three standard citation networks benchmark datasets used for semi-supervised learning evaluation [44]. In these citation networks, nodes represent publications, edges denote citation, the input feature matrix are bag of words and label matrix contain the class label of publication. We use the same data format as GCN, i.e., 20 labels per class in each citation network.

Directed networks We evaluate our method on four directed networks - IEEE 118-bus system (IEEE bus), ACTIVSg200, ACTIVSg500, and ACTIVSg2000 [8, 7, 25]. For IEEE 118-bus system, we consider a (unweighted-directed) graph as a model for the IEEE 118-bus system where nodes represent units such as generators, loads and buses, and edges represent the transmission lines. The input features of power grid network are generator active power upper bound (PMAX) and real power demand (PD) obtained from MATPOWER case struct. For ACTIVSg200, ACTIVSg500, and ACTIVSg2000, we also treat them as unweighted directed power grid networks. In particular, the input features are: (i) real power demand (PD); (ii) reactive power demand (QD); (iii) voltage magnitude (VM); (iv) voltage angle (VA); (v) base voltage (BASE_KV). For the power grid networks, we test them with 10% label rate for training set, 20% for validation and 70% for test sets. Summary statistics of the data are summarized in Table 3.

C.2 Training Settings

For all experiments, we train our model utilizing Adam optimizer with learning rate $lr_1 = 0.01$ for undirected networks and $lr_2 = 0.1$ for directed networks. We use the same random seeds across all models (the experiments are repeated 5 times, each with the same random seed). To prevent over-fitting, we consider both adding dropout layer before two graph convolutional layers and kernel regularizers (ℓ_2) in each layer. For undirected networks, we set the parameters of baselines by using two graph convolutional layers with 16 hidden units, ℓ_2 regularization term with coefficient 5×10^{-4} , and dropout probability p_{drop} of 0.5 (for ARMA, except for number of hidden units, the hyperparameters setting are significantly different from others). For directed networks, we consider using a two-layer network but with n_h^{SOA} hidden units (where $n_h^{SOA} \in \{16, 32, 64, 128, 256\}$), learning rate lr_2 with 0.001, 0.5 dropout rate and ℓ_2 regularization weight of 5×10^{-4} for baselines (for MotifNet, except for number of hidden units, the hyperparameters setting are significantly different from others). The best hyperparameter configurations, including dropout rate p_{drop} , optimal number of hidden neurons $n_h^{TRI-GNN}$, regularization parameter μ , the coefficient \mathcal{R} (i.e., related to the number

of power iteration steps), element-wise nonlinear activation function $\sigma(\cdot)$, of TRI-GNN for each dataset by using standard grid search mechanism (the optimal kernel regularization weight ℓ_2 always equal to 5×10^{-4}). In STAN module, for the weighting factor $\alpha(u)$, we choose the best setting for each model, where $\alpha(u)$ is searched in $\{0.0, 0.1, 0.2, 0.3, 0.4, 0.5\}$; for the number of STAN iterations \mathcal{T} , we search \mathcal{T} from $\{0, 1, 2\}$. We also use a parallel structure by stacking multiple convolution based TRI-GNN layers to attenuate the noise issue. For the choice of k in the k -hop neighborhood, (i) for citation networks: we search k from $\{1, 2, 3\}$ (where $k_{\text{Cora-ML}} = 2$, $k_{\text{CiteSeer}} = 1$, and $k_{\text{PubMed}} = 1$) and (ii) for synthetic power networks: we search k from $\{3, 4, 5\}$ (where $k_{\text{IEEE}} = 5$, $k_{\text{ACTIVSg200}} = 5$, $k_{\text{ACTIVSg500}} = 3$, and $k_{\text{ACTIVSg2000}} = 5$). For threshold hyperparameters of topology-induced multiedge construction, in practice, we select the ϵ_1 and ϵ_2 values based on quantiles of Wasserstein distances between persistence diagrams. The optimal choice of ϵ_1 and ϵ_2 can be obtained via cross-validation. Specifically, we first search ϵ_1 from $\{0.05, 0.1, 0.15, 0.2\}$ -quantiles. With the best selection of ϵ_1 , we then search ϵ_2 from $\{0.1, 0.15, \dots, 0.95\}$ -quantiles. Note that some most recent studies of [43, 14] have shown that dropping out edges helps reducing over-smoothing and improves training efficiency.

Running Time We report results for the average time (in seconds) taken for PD generation from k -hop neighborhood subgraph (in our experiment, $k \in \{1, 2, 3, 5\}$) and the average training time (in seconds) per epoch of TRI-GNN_A for both undirected and directed networks on Tesla V100-SXM2-16GB.

Table 4: Complexity of TRI-GNN_A: the average time (in seconds) to generate PD and training time per epoch.

Dataset	PD generation TRI-GNN _A (per epoch)	
IEEE 118-Bus	5×10^{-4} s	0.01s
ACTIVSg200	5×10^{-4} s	0.01s
ACTIVSg500	1×10^{-3} s	0.02s
ACTIVSg2000	1×10^{-2} s	0.25s
Cora-ML	7×10^{-2} s	0.05s
CiteSeer	1×10^{-2} s	0.35s
PubMed	2×10^{-1} s	0.30s

C.3 Ablation Study of TRI-GNN_A

The extended ablation study with statistical significance (i.e., z -test between TRI-GNN_A and baselines) is in Table 5. Except for the PubMed (the reason maybe that the PubMed is a very sparse network), in the power grids and Cora-ML, all TRI-GNN components are highly statistical significant, but in CiteSeer individual contributions of TIMR is statistical significant, while STAN is non-significant. This can be explained by CiteSeer highest sparsity and richest set of node attributes. Overall, TIMR is universally important.

Table 5: Ablation study of TRI-GNN_A in accuracy (%) and standard deviation (%) in (); *, **, *** denote p -value $< 0.1, 0.05, 0.01$ (i.e., significant, statistically significant, highly statistically significant).

Dataset	TRI-GNN _A	TRI-GNN _A	TRI-GNN _A
	w/o Ω	w/o STAN	with Ω, STN
IEEE 118-Bus	*82.20 (1.68)	*82.38 (2.00)	*82.21 (1.88)
ACTIVSg200	***82.75 (2.09)	**84.56 (1.75)	***82.80 (2.73)
ACTIVSg500	*97.85 (0.56)	*97.69 (0.63)	*97.54 (0.72)
ACTIVSg2000	*88.59 (0.60)	*88.82 (0.56)	*88.63 (0.65)
Cora-ML	***84.33 (0.63)	***84.63 (0.61)	***84.42 (0.70)
CiteSeer	73.25 (0.70)	*73.10 (0.70)	*73.10 (0.63)
PubMed	79.77 (0.51)	79.71 (0.50)	79.68 (0.63)

C.4 Random Attacks

Here we present the results for TRI-GNN_D under random attacks. As demonstrated in Figure 7, we can see that the TRI-GNN_D architecture indeed is capable to capture much richer local and global higher-order graph information. Particularly on Cora-ML, the performance of the 4 baselines drop rapidly as the ratio of perturbed edges increases, while TRI-GNN_D successfully defends against the perturbations. Overall, the robustness of TRI-GNN_D and TRI-GNN_A (see Figure 4 in the main manuscript) are similar. These results indicate that the new TRI-GNN architecture with both types of the considered filtration functions is a highly competitive alternative for graph learning under adversarial perturbations.

C.5 Diverse Set of TRI-GNN

We experimented shorter training sets and numbers of layers (see Table 6). TRI-GNN sustains its competitiveness, yielding one of the best results even under 20% reduction of the training set (compare Table 1 in the main manuscript). Higher order holes have not brought up any noticeable improvement as higher order homology are almost not met in relatively small node neighborhoods.

Table 6: TRI-GNN_D with different training set sizes and number of layers. Number of runs is 50.

Cora-ML	Training set size			
	100% Train	90% Train	80% Train	50% Train
Accuracy (%) (std)	84.98 (0.49)	84.15 (0.55)	84.00 (0.64)	73.20 (0.50)
Cora-ML	Layers			
	2 layers	8 layers	16 layers	32 layers
Accuracy (%) (std)	84.98 (0.49)	80.70 (0.75)	78.06 (1.07)	72.87 (1.30)

C.6 Comparison with GCN-LPA, NodeNet, and DFNet-ATT

Tables 7 and 8 compare the performance of TRI-GNN_D to other state-of-the-art graph classification baselines, i.e., DFNet-ATT [54], GCN-LPA [52], and NodeNet [18]. On Cora-ML[†], we follow the settings of NodeNet, i.e., we split the Cora-ML dataset into training (80%) and test sets (20%). We can observe that TRI-GNN significantly outperforms GCN-LPA, NodeNet, and DFNet-ATT on these datasets.

Table 7: Average accuracy (%) and standard deviation (%) in () on Cora-ML, ACTIVSg200, and ACTIVSg500.

Method	TRI-GNN _D	NodeNet
Cora-ML [†]	85.85 (0.71)	84.03 (0.40)
ACTIVSg200	86.18 (0.20)	80.15 (0.91)
ACTIVSg500	98.11 (0.43)	95.00 (0.50)

Table 8: Average accuracy (%) and standard deviation (%) in () on Cora-ML and CiteSeer.

Method	TRI-GNN _D	GCN-LPA	DFNet-ATT
Cora-ML	84.98 (0.49)	81.68 (0.93)	84.65 (0.50)
CiteSeer	73.32 (0.48)	71.40 (0.60)	70.18 (0.71)

C.7 Additional Results

We also evaluate our methods on two relatively large datasets, i.e., ogbn-products and ogbn-arxiv. Table 9 below shows that our proposed TRI-GNN always outperforms state-of-the-art methods in terms of classification accuracy on large networks. The results also indicate that our proposed model is capable to achieve highly promising results on very large networks.

Table 9: Average accuracy (%) and standard deviation (%) in () on ogbn-products, and ogbn-arxiv.

Method	TRI-GNN _D	GCN	GAT	RGCN	APPNP
ogbn-products	84.00 (0.007)	78.87 (0.003)	80.02 (0.001)	81.35 (0.005)	83.17 (0.006)
ogbn-arxiv	74.30 (0.003)	72.18 (0.002)	72.47 (0.002)	72.97 (0.001)	72.10 (0.003)

C.8 Boundary Sensitivity on ACTIVSg500

We also evaluate the boundary sensitivity of hyperparameters ϵ_1 and ϵ_2 on ACTIVSg500 dataset. The results are presented in Figure 8. We can observe that, compared with ϵ_2 (i.e., removing existing edges based on topological similarity among two node neighborhoods), TRI-GNN is more sensitive to ϵ_1 (i.e., adding edges If two nodes in \mathcal{G} are topologically similar).

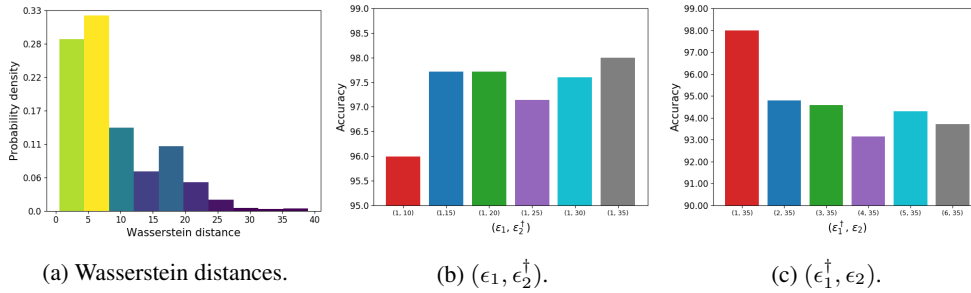


Figure 8: Hyperparameters ϵ_1 and ϵ_2 selection of TRI-GNN on ACTIVSg500 dataset.